Available online at www.sciencedirect.com
SCIENCE DIRECT®
International Journal of Solids and Structures 42 (2005) 697–715
INTERNATIONAL JOURNAL OF SOLIDS and STRUCTURES
www.elsevier.com/locate/ijsolstr

Dynamic mechanical and fracture properties of an infiltrated TiC-1080 steel cermet

D. Rittel [a,*], N. Frage [b], M.P. Dariel [b]

[a] *Faculty of Mechanical Engineering, Technion, Israel Institute of Technology, 32000, Haifa, Israel*
[b] *Department of Materials Engineering, Ben-Gurion University of the Negev, Beer-Sheva, Israel*

Received 14 April 2004
Available online 6 August 2004

Abstract

The dynamic mechanical and fracture properties of a TiC porous network infiltrated with 1080 steel are reported. Following infiltration, the cermet is subjected to various heat treatments that affect essentially the steel matrix. Dynamic compression tests show that the heat treatments increase the fracture strength of the cermet. The quasi-static fracture toughness (K_{Ic}) is also increased by the heat treatments. The dynamic (initiation) fracture toughness (K_{Id}) is substantially higher (by about a factor of 3) than its static counterpart. Failure mechanisms consist mainly of cleavage of the TiC and matrix grains, along with minor interfacial decohesion. However, dynamic loading induces substantial damage around the crack tip, consisting essentially of cleavage of TiC grains. Microcrak toughnening is believed to be responsible for the high dynamic toughness of the material. The critical microstructural fracture event is thus identified as the spreading of TiC cleavage microcracks into the neighboring steel grains.

Keywords: TiC-steel cermet; Dynamic fracture; Microcrack toughnening; Cleavage

1. Introduction

The mechanical properties of various cermets, with emphasis on SiC–Al systems, have been extensively studied. The characterization of the mechanical and fracture properties of this (and similar) cermets focuses generally on the static mechanical properties and fracture toughness (K_{Ic}) of the material, including the influence of the composition and microstructure (for a review on metal-matrix composites, see e.g., Taya and Arsenault, 1989). Particulate reinforced composites have long been investigated and sophisticated

* Corresponding author. Tel.: +972 4 8293261; fax.: +972 4 8324533.
E-mail address: merittel@tx.technion.ac.il (D. Rittel).

0020-7683/$ - see front matter © 2004 Elsevier Ltd. All rights reserved.
doi:10.1016/j.ijsolstr.2004.06.027

models have been developed to relate their toughness and microstructure (see e.g., Sigl and Fischmeister, 1988; Budiansky et al., 1988; Sigl et al., 1988; Lloyd, 1991). Most of the work has concentrated on quasi-static properties, so that relatively little is available on the dynamic mechanical and fracture properties of these cermets. This information is nevertheless of prime importance since dynamic loading situations are currently encountered in structural applications. Concerning TiC reinforced steel composites, it appears that the subject has been addressed long ago, as can be noted in a recent review paper by Parashivamurthy et al. (2001). Again, however, it can be noted that the main interest in this cermet lies in its tribological properties. Therefore, the mechanical and fracture properties, with emphasis on high rates of loading for which little information is available especially concerning dynamic fracture still need to be investigated. The dynamic response to planar impact of these cermets has been studied recently by Klein et al. (2003). The authors determined the Hugoniot elastic limit and the spall strength of the material at strain rates of the order of 10^4 s^{-1}. A model was proposed to account for the confining effect of the steel matrix on the ceramic particles.

The present paper presents new results on the dynamic mechanical and fracture behavior of infiltrated TiC-1080 steel cermets, to be compared with available data on the static properties of these materials. Novel results on the fracture properties of the cermets are reported, expressed in terms of the static fracture toughness (K_{Ic}) and its dynamic counterpart (K_{Id}). For the various tests, the failure mechanisms are described, and a comparison between the static and dynamic properties of the cermets is established and discussed.

The paper is organized as follows. First we present the investigated cermets, their fabrication process and resulting microstructure. Next, the various non-standard experimental procedures are described to get the reader more familiar with dynamic testing. The next section reports experimental results, starting with high-rate impact. The following section deals with quasi-static and dynamic fracture properties of the cermets. The failure micromechanisms are then presented, followed by a comprehensive discussion of the results.

2. Material preparation and microstructure

An important consideration in the choice of the cermet was the possibility of investigating, the influence of the state of the metallic component on its dynamic response, an effect that had not been systematically investigated so far. The selected cermet is a TiC-carbon steel composite. Although the dynamic properties of dense TiC ceramics are not high, they present some definite advantages. Ceramic TiC matrices with controlled open porosity (preforms) can be manufactured easily. Moreover, owing to the good wetting of TiC by molten steel, the porous preforms can be completely infiltrated by the molten metal. By varying the heat treatment applied to the cermet, the state of the metallic component can be changed while that of the ceramic matrix is kept constant.

The titanium carbide-steel cermets, subject of this study, consisted of two interpenetrating and interconnected, ceramic and metal networks. They were fabricated by infiltrating a porous TiC preforms with molten 1080 carbon steel. Titanium carbide, (CERAC®, Cat. No. T-1151, 325 mesh) powder was compressed at 35 MPa and sintered at 1600 °C for 60 min in a graphite furnace. At the outcome of this treatment, and as long as the same initial powder was used, reproducible preforms were obtained with roughly 30% total porosity. The porosity, practically all of it open, was determined by the liquid displacement method in distilled water. Infiltration by molten steel was carried out under vacuum of 10^{-4} Torr at 1500 °C for 30 min, followed by furnace cooling. The thermal treatment of the infiltrated TiC-steel cermets consisted of an austenitizing treatment of the samples, sealed in evacuated quartz capsules, for 1 h at 870 °C, followed by furnace cooling or immersing and shattering the capsules in water. Tempering the quenched cermets was done in air at 300 and 400 °C respectively, for 1 h. Four different conditions were therefore investigated. They are denoted according to their heat treatment. ''AS'', ''T300'', ''T400'' and ''Quenched'' stand

for as-received (furnace cooled), quenched and tempered at 300 °C, quenched and tempered at 400 °C and quenched respectively.

The AS samples, etched with a Nital solution, displayed a clearly pearlitic microstructure of the metallic component. The TiC-steel interface was very smooth, indicating some dissolution on the ceramic in the metallic melt during infiltration. In the Quenched samples, the pearlitic microstructure of the metallic regions was replaced by a fine plate-like structure, reminiscent of high-carbon martensite (see Klein et al., 2003). The resolution of the X-ray diffraction patterns did not reveal split diffraction peaks characteristic of martensite, possibly because of the low relative metallic fraction.

3. Experimental

Two kinds of specimens were manufactured, according to their destination. Cylindrical specimens (typically 5.5, 3.3 mm height) were prepared for uniaxial dynamic compression. Small, square-sectioned beams were prepared for the fracture mechanics (static and dynamic) experiments. The dimensions of each beam varied, since they were manufactured individually and not serially. Typical dimensions are 5.5 mm (thickness) × 5.0 mm (height) for the cross-section, and 40.0 mm for the length. A notch was introduced at mid-bar length with a 0.15 mm thick diamond blade. The notch root radius is estimated to be of the order of 0.2 mm. The relative depth of the notch was in the range of 0.4–0.5.

Dynamic compression was carried out on a Kolsky (Split Hopkinson pressure) bar (see e.g. Kolsky, 1963). Two sets of bars were used, according to the experiment. Dynamic compression was carried out using 12.7 mm diameter heat treated MAR250 steel. The transmitter bar is shorter than the incident to allow for pulse trapping. This procedure avoids repeated pounding of the specimen by the waves trapped in the bars. Dynamic fracture experiments were carried out using a single instrumented 12.7 mm diameter 7075-T6 aluminum alloy. The bar signals were processed according to the standard procedure, into which signal dispersion is accounted for, according to Lifshitz and Leber (1994). In these tests, the quality of the signals was excellent, so that there was no need to instrument the specimen itself as in Ramesh and Ravichandran (1990).

The quasi-static fracture toughness—K_{Ic}—was measured by three-point bending of the notched bars, on an MTS 810 servo-hydraulic testing machine, under displacement control. The crosshead velocity was fixed to 0.083 mm/s. A two-dimensional finite element model (plane-strain) was run on ANSYS (1994) finite element code. For each specimen tested, the stress intensity factor corresponding to unit load was calculated. The fracture toughness was thus determined by multiplying the unit stress intensity factor by the maximum (fracture) load.

The dynamic fracture toughness—K_{Id}—was determined from one-point impact bend tests. The procedure has been described in detail, e.g., in Weisbrod and Rittel (2000), and its validity has been assessed e.g., in Rittel and Weisbrod (2001), and Rittel et al. (2002a). For the sake of brevity, we will only outline the main characteristics of the procedure. The main idea is that, based on the linearity of the fracture process (LEFM assumptions), the evolution of the stress intensity factor(s) can be determined if the loading force is known, and if the response of the structure to unit impulse is determined. In other words, if the applied load $F(t)$ is determined from a one-point impact test, and if $k_\delta(t)$ is the stress intensity resulting from unit impulse, then the evolution of the stress intensity factor is given by:

$$K(t) = F(t) * k_\delta(t) \tag{1}$$

where the $*$ sign indicates a time convolution integral. Therefore, if the fracture time—t_{frac}—is determined, the fracture toughness is the value of the stress intensity factor at fracture, i.e.

$$K_{\mathrm{Id}} = K(t)@t = t_{\mathrm{frac}} \tag{2}$$

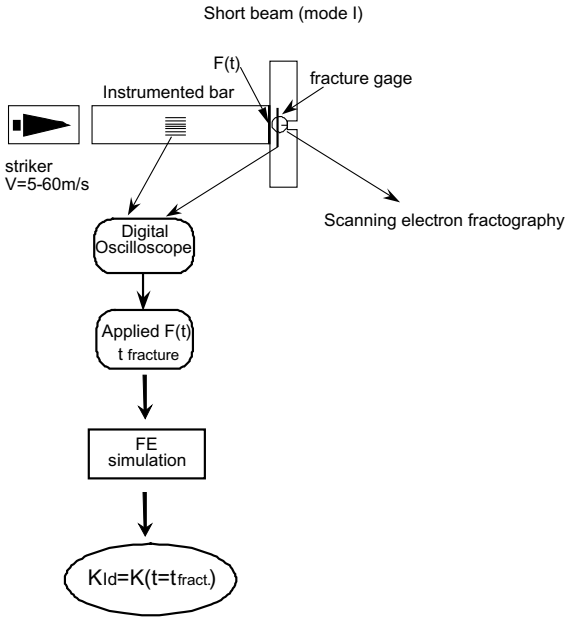

Fig. 1. Schematic representation of a one-point impact test for dynamic fracture toughness determination. The unsupported specimen is impacted symmetrically, and the onset of crack propagation is detected by means of single wire fracture gages.

A schematic representation of the setup is given in Fig. 1. For dynamic fracture testing, we used, as mentioned above, a single 7075-T6 bar which was observed to yield higher quality signals than a MAR250 bar. The quality of the signals is dictated by mechanical impedance matching, and in each case, the specimen geometry dictates the final choice of the bar. The specimen is instrumented by 2 single wire fracture gages (MM CD 02 15A), one on each side of the specimen. The gages are positioned as closely as possible to the crack-tip. It should be noted that, whereas detection of fracture is a crucial issue in such experiments, the use of single wire fracture gages gives an accurate indication of the onset of crack propagation, as shown for small beam specimens (Weisbrod and Rittel, 2000) and regular Charpy size beams (Rittel et al., 2002a). From a practical point of view, the specimen fractures due to its sole inertia. As it is unsupported during the test, numerical modeling is greatly simplified in terms of boundary conditions. The dynamic unit impulse response was calculated by a 2D (plane strain) elastodynamic finite element model of the specimen (ANSYS, 1994). The applied load was calculated from the incident and reflected pulses (ε_{in} and ε_{ref}) measured on the instrumented bar, according to:

$$F(t) = AE[\varepsilon_{in}(t) + \varepsilon_{ref}(t)] \tag{3}$$

where A and E are the bar cross section and Young's modulus respectively.

In these tests, the sample size was relatively large initially. However, when crack extension was observed to proceed on a slant plane, as opposed to linear extension of the notch, the test was considered as invalid, as it involved mixed-mode fracture. The reported results pertain to those only tests for which the fracture path was an extension of the preexisting notch. The typical valid sample size was therefore at least 15 specimens per grade, on the average.

Statistical data processing was applied as follows. Firstly, the results obtained for the various groups (heat treatments) were compared using Laplace's statistical estimate. This comparison answered the question as to whether the groups can be differentiated. Next, the bootstrap algorithm was used to smooth the

plots, and recalculate the average value and standard deviation, based on a sample size of $n = 1000$ (Efron, 1979).

Failure mechanisms were assessed using standard metallographic procedures and scanning electron microscopy (JEOL, JSM 840).

4. Experimental results

4.1. Static mechanical properties

The hardness was determined in a Buehler micro-hardness tester using a Vickers indenter under a 20 N load. The acoustic wave velocity was determined from direct measurement of the travel time of longitudinal and transverse waves, generated by corresponding 5 MHz probes. Young's (E), and shear (G) elastic moduli, were derived from the longitudinal and transverse ultrasound velocities. A detailed account of the mechanical properties of the cermet can be found in Klein et al. (2003). For the sake of brevity, we will just mention that Young's modulus of the cermet varied with its condition, typically from 358GPa (T400) to 367 GPa (AS). The hardness level varied from HV1080 (AS) to HV1750 (Quenched) through HV1350 (T300). The fracture strength was determined by three-point bending of 3 mm × 4 mm × 20 mm beams. The prescribed cross head velocity was 0.5 mm/min. The sample size comprised 10 specimens. The measured fracture stress was 1430 ± 19 MPa for AS, 763 ± 12 MPa for Quenched, 936 ± 13 MPa for T300 and 990 ± 12 MPa for T400. It should be mentioned that these results provide limited information on the tensile strength of the materials, due to the nature of the test. Yet, it is readily seen that the thermal treatment affects both the hardness and the rupture strength of the investigated cermets.

4.2. Dynamic compression properties

A typical signal, as recorded on the Kolsky apparatus is shown in Fig. 2a. The signals clearly indicate that the majority of the incident signal is transmitted through the specimen. Fig. 2b shows the loads exerted on both sides of the cylindrical specimen, after data reduction. The two forces are very similar, indicating a state of dynamic equilibrium in the specimen. In most cases, the stress–strain curves indicated a clear maximum level, taken as the failure stress of the material (Fig. 3a). However, in certain cases, the stress–strain showed a narrow plateau, followed a subsequent peak. In this case (Fig. 3b), the first plateau was taken as the failure stress. This phenomenon is deemed to be related to the failure process in which multiple cracking develops (Rittel, 2000).

Fig. 4 summarizes the dynamic compression strength of the four various heats. This plot has been prepared after bootstrap statistical processing of the data. It should be emphasized that this process only smoothens the data without altering whatsoever its nature. This figure shows that the Quenched and T300 conditions are distinctly different from the two other AS and T400 conditions. The results suggest that the quenched condition possesses a superior strength with respect to all other conditions. Table 1 summarizes the various strength related parameters, as measured, and as modeled using the bootstrap technique. Further insight is gained by comparing the groups, based on Laplace statistics, as shown in Table 2. This comparison confirms that the conditions of AS and T400 cannot be distinguished with a level of confidence of 90%.

4.3. Quasi-static fracture toughness—K_{Ic}

All the experimental results reported below were obtained at room temperature in ambient air. A typical load–displacement plot is shown in Fig. 5. The machine compliance has not been corrected in this plot, thus

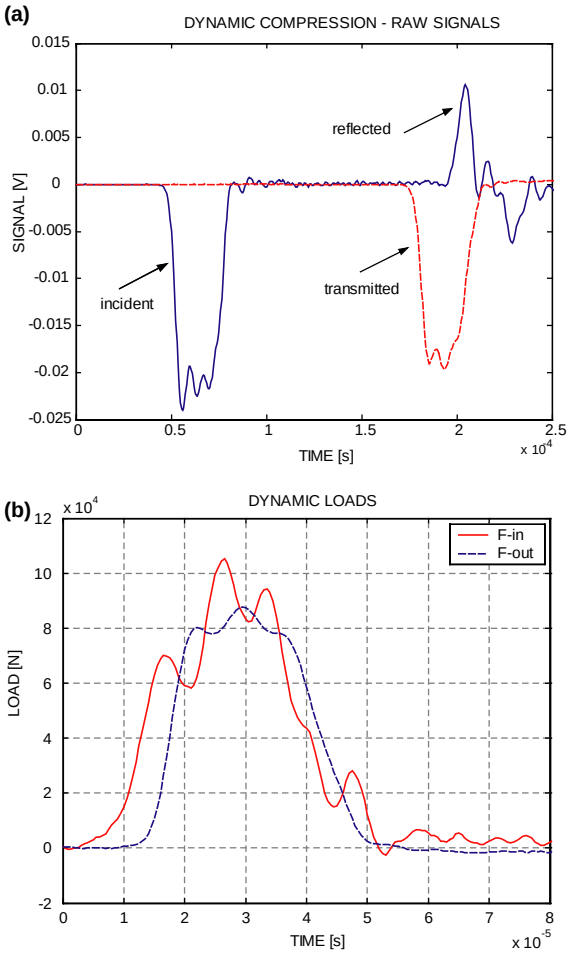

Fig. 2. Typical output of a dynamic compression test with the Kolsky apparatus: (a) Raw signals from the strain gages on the bar. An incident compressive signal is partly reflected, partly transmitted through the cylindrical specimens. These signals are used to determine the loads and displacements applied to the specimen. (b) Processed signals showing the loads on each side of the specimen. The similarity indicates a state of dynamic equilibrium.

causing some slight nonlinearity until fracture. However, the only needed information is the maximum (failure) load. All the specimens failed in the abrupt fashion shown in Fig. 5. A summary of the quasi-static fracture toughness values is given in Table 3(panels A and B), for the various heats. Fig. 6 shows a histogram plot of the data. Here too, the average values of the fracture toughness can be compared using Laplace's criterion, as shown in Table 4. The results essentially indicate that T300, T400 and Quenched conditions are distinct from the AS condition. However, T300, T400 and Quenched conditions are not distinct one from another, as opposed to the AS condition. It should be noted that for T300 condition, the fracture toughness values exhibit a higher degree of scatter.

Moreover, the results indicate that the fracture toughness of all the cermets is relatively high, due to the presence of the metallic binder. It also appears that the various heat treatments all increase the fracture toughness of the material, to various extents. To conclude this section, the results show that heat treatments confer an increased fracture toughness to the investigated material.

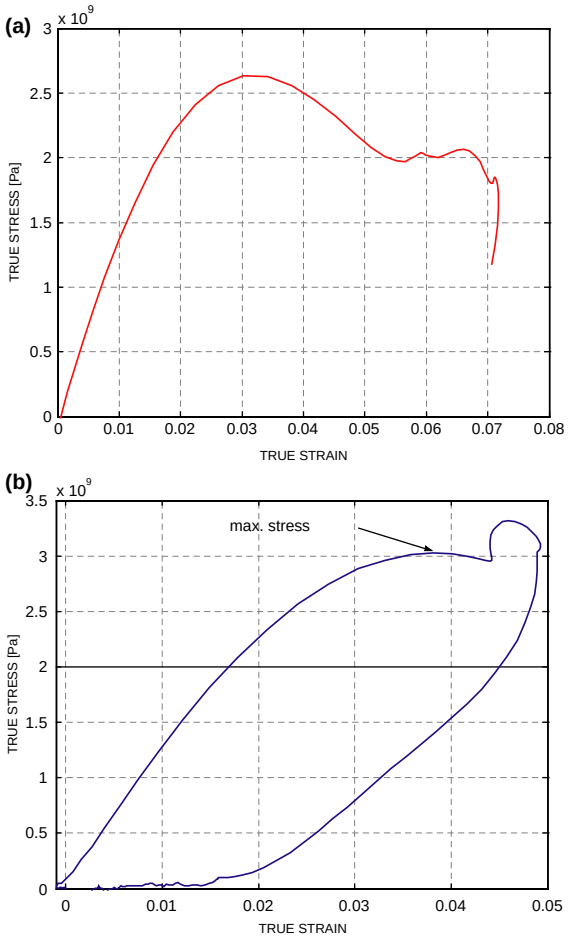

Fig. 3. Typical dynamic stress–strain curves. (a) Stress–strain curve followed by specimen fracture. (b) Stress–strain curve followed by specimen unloading. The plateau stress is taken as the maximal stress, whereas the rest of the curve may be related to incomplete fracture prior to unloading.

4.4. Dynamic fracture toughness—K_{Id}

Similar to the quasi-static fracture toughness, the dynamic fracture toughness results are presented in Table 5(panels A and B). Fig. 7 shows a histogram plot of the data. A comparison of the average dynamic fracture toughness values is given in Table 6. It can first be noted that the dynamic fracture toughness of *all conditions* is clearly superior to the static fracture toughness. In fact, K_{Id} is on the average equal to 3 times K_{Ic}. From Fig. 7 and Table 5, it appears that, compared with the quasi-static fracture toughness, the dynamic fracture toughness values are much less widespread. It also seems that the T300 and T400 conditions are not distinguishable one from another, while they are distinct from the AS condition. Fig. 7 essentially shows that all three Quenched, T300 and T400 conditions possess comparable levels of dynamic fracture toughness levels, as opposed to the AS condition.

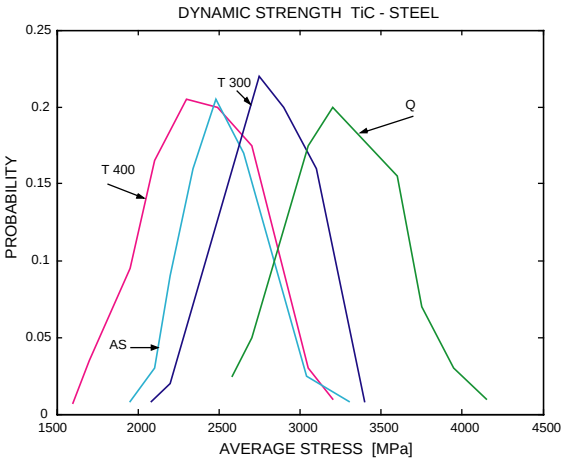

Fig. 4. Histograms showing the dynamic strength of the cermet subjected to various heat-treatments.

Table 1
Summary of the dynamic compression tests

Group	Array	σ_{aver} (MPa)	σ_{max} (MPa)	σ_{min} (MPa)	Model	σ_{aver} (MPa)	σ_{max} (MPa)	σ_{min} (MPa)
AS	7	2468	2860	2076	1000	2463	2957	1945
T300	10	2817	3150	2000	1000	2811	3543	2032
T400	10	2399	3116	1930	1000	2402	3207	1593
Quenched	9	3312	3715	2600	1000	3327	4229	2507

The array column indicates the experimentally recorded values, with the average stress and its limits. The model column and thereon indicate results from the bootstrap process. Note that while it smoothens the data, the bootstrap process does not alter the stress values.

Table 2
Comparison of the various fracture strength values

*	AS	T300	T400	Quenched
AS	*	2.23	0.43	4.68
T300		*	2.50	2.64
T400			*	4.80
Quenched				*

Laplace criterion ($Z_L = 1.65$) and confidence level of 90%. All values $Z > Z_L$ indicate that the groups can be differentiated.

4.5. Quasi-static fracture toughness—K_{Ic} at low temperature

In order to gain additional understanding on the relation between quasi-static and dynamic fracture behavior, a limited series of experiments was carried out at low temperature. Specifically, a set of 3 point-bend specimens, identical to those used previously was tested for K_{Ic} determination. All the specimens were soaked for 30 min in liquid nitrogen and tested 1minute after extraction from the bath. The specimen temperature was not determined accurately, but in view of the poor thermal conduction of the predominant ceramic phase, the temperature was probably quite low, of the order of 100 °C. The results are summarized in Table 7. The small sample size does not allow for any statistically meaningful conclusion to be drawn.

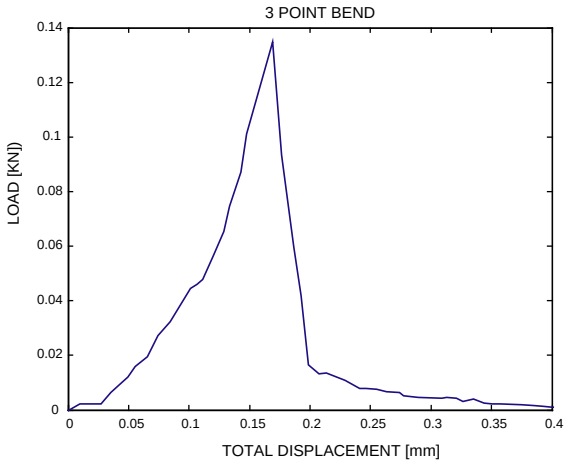

Fig. 5. Typical load–displacement record of a three point bend test used to determine K_{Ic}. Note that the machine compliance has not been corrected.

Table 3
Summary of results for the quasi-static fracture toughness K_{Ic} (panels A and B)

Group	Array	K_{Ic} average + 90% CI ($MPa\,m^{1/2}$)	K_{Ic} max ($MPa\,m^{1/2}$)	K_{Ic} min ($MPa\,m^{1/2}$)	Span ($MPa\,m^{1/2}$)	SD ($MPa\,m^{1/2}$)
Panel A: Experimental data[a]						
AS	7	9.1–**11.0**–13.0	17.0	6.1	10.9	3.6
T300	5	15.4–**20.3**–25.2	28.4	11.7	16.7	7.1
T400	6	13.4–**16.1**–18.9	22.4	11.1	11.3	4.5
Quenched	5	17.9–**19.7**–21.4	23.2	16.6	6.6	2.5
		K_{Ic} average				
Panel B: Bootstrap model of 1000 sample size						
AS	1000	**11.0**	17.1	4.5	12.6	2.3
T300	1000	**20.3**	32.5	7.8	24.7	4.4
T400	1000	**16.1**	24.3	8.1	16.2	2.7
Quenched	1000	**19.7**	23.7	8.3	8.3	1.5

[a] The average value of K_{Ic} is given (in boldface) with a 90% confidence interval according to Student's criterion.

However, it clearly appears that the toughness values obtained at low temperature are quite similar to those obtained at room temperature.

4.6. Fractographic analysis

Prior to characterizing the various fracture surfaces of each type of specimen, the basic fractographic features were characterized, using energy dispersive X-ray analysis in the scanning electron microscope. A typical output from a line scan is show in Fig. 8, for an AS impact specimen (#8). This figure illustrates the difficulty in clearly identifying the TiC particles from the 1080 steel matrix. However, several examinations revealed that the TiC grains fail essentially by cleavage, with well defined facets. The failure mechanism of the matrix (slightly brighter) shows no well defined dimples. Rather, it exhibits relatively flat featureless facets that suggest cleavage as the operating failure mechanism (see, e.g. Metals Handbook,

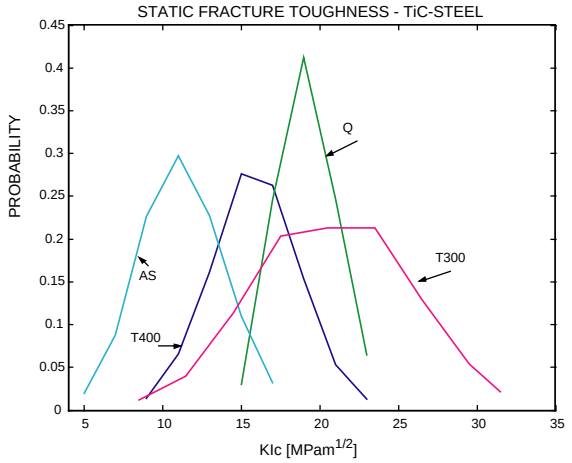

Fig. 6. Histograms showing the quasi-static fracture toughness—K_{Ic}—of the cermet subjected to various heat-treatments. Note the relative scatter of the data.

Table 4
Comparison of the various average quasi-static fracture toughness values

*	AS	T300	T400	Quenched
AS	*	**2.66**	**2.24**	**4.89**
T300		*	1.14	0.174
T400			*	**1.69**
Quenched				*

Laplace criterion ($Z_L = 1.65$) and confidence level of 90%. All values $Z > Z_L$ indicate that the groups can be differentiated (boldface).

Table 5
Summary of results for the dynamic fracture toughness K_{Id} (panels A and B)

Group	Array	K_{Id} average + 90% CI (MPa m$^{1/2}$)	K_{Id} max (MPa m$^{1/2}$)	K_{Id} min (MPa m$^{1/2}$)	Span (MPa m$^{1/2}$)	SD (MPa m$^{1/2}$)
Panel A: Experimental data[a]						
AS	15	47.2–**51.9**–56.5	74.0	27.3	46.7	13.4
T300	21	61.1–**68.0**–74.9	113.8	36.0	77.8	23.9
T400	22	57.2–**64.5**–71.4	121.8	17.3	104.5	26.3
Quenched	11	49.2–**58.9**–68.7	108.3	21.8	86.5	23.8
		K_{Id} average				
Panel B: Bootstrap model of 1000 sample size						
AS	1000	**51.6**	80.1	21.7	58.5	10.7
T300	1000	**68.2**	126.4	8.9	117.6	21.2
T400	1000	**64.4**	129.7	8.0	121.6	21.8
Quenched	1000	**59.2**	111.4	9.0	102.4	17.4

[a] The average value of K_{Ic} is given (in boldface) with a 90% confidence interval according to Student's criterion.

1974). In addition, the steel matrix can also be observed to fail by interfacial decohesion from the TiC particles, to a lesser extent. All the grades were thoroughly examined for both quasi-static and dynamic

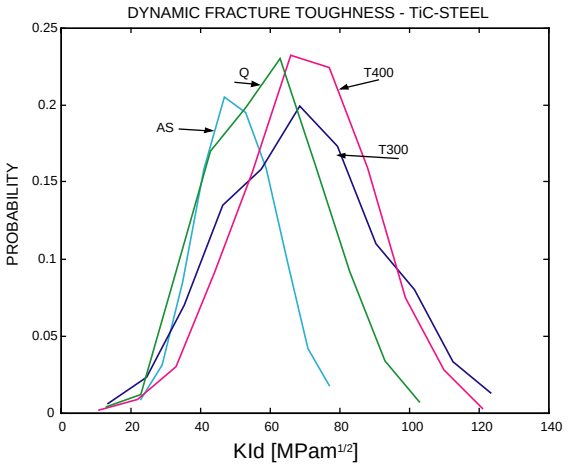

Fig. 7. Histograms showing the dynamic fracture toughness—K_{Id}—of the cermet subjected to various heat-treatments. Note the relative clustering of the data.

Table 6
Comparison of the various average dynamic fracture toughness values

*	AS	T300	T400	Quenched
AS	*	**2.57**	**1.91**	0.88
T300		*	0.46	1.02
T400			*	0.61
Quenched				*

Laplace criterion ($Z_L = 1.65$) and confidence level of 90%. All values $Z > Z_L$ indicate that the groups can be differentiated.

Table 7
Quasi-static fracture toughness of selected specimens tested at low temperature, 1 min after extraction from a liquid N2 bath

Treatment	K_{Ic} (MPa m$^{1/2}$)
Q	18.1
T300	16.7
T300	14.1
T300	15.7
T400	16.9
T400	14.9

loading. However, for the sake of brevity, we will only present selected fractographs of fracture mechanics specimens. Typical fractographs of room temperature fracture, both quasi-static and dynamic, are shown in Figs. 9 and 10, respectively. These figures show essentially cleavage of the TiC and steel grains, regardless of the heat treatment and loading rate. Therefore, one cannot differentiate static fracture from dynamic fracture on a sole fractographic basis. Fig. 11 shows a typical fractograph of low temperature quasi-static fracture. Here too, the above-mentioned micromechanisms operate without any particularity related to low temperature failure. To summarize, the fractographic examination *did not* indicate a specific difference between the various grades, type of loading and test temperature.

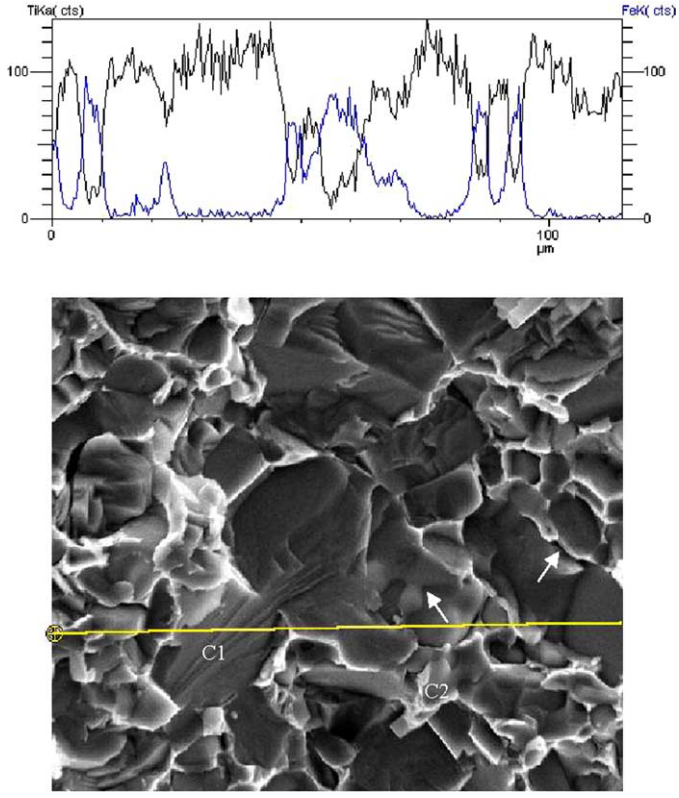

Fig. 8. Energy Dispersive X-ray line scan on a fracture surface. The failure mechanisms consist of TiC grain cleavage (C1), interfacial decohesion (D) and cleavage of the steel matrix (C2).

4.7. Damage analysis

Longitudinal metallographic sections, perpendicular to the fracture plane, were prepared to assess the nature of the damage related to the crack initiation process, and its rate. Fig. 12 shows a typical metallographic section of a T300 specimen that was fractured under quasi-static conditions. It can be noted that the material below the fracture plane is unaffected by the fracture process. Both the TiC and the steel matrix grains lying below the fracture plane are intact, close to the notch-tip and further along the crack path. Fig. 13 shows a metallographic section for the same material that has been fractured dynamically. Here, the results are dramatically different. Numerous cleavage microcracks are observed to develop in the vicinity of the notch. All the cracks are located in the TiC grains without observable damage in the steel matrix. The morphology of the damage comprises cracks that extend across a few TiC grains, others that confine to one grain only, and also multiple short cracks within the same TiC grain. The microcracks are detected up to a few grains below the fracture plane. The dimensions of the damaged zone are of the order of 15 μm deep (below fracture plane) and some 60 μm along the crack path. Careful examination did not reveal such extensive microcracking farther away from the crack origin. These observations indicate that the dynamic initiation process affects the neighborhood of the crack (notch)—tip by creating several cleavage microcracks in the TiC grains, all of which are located near the crack-tip. A detailed TEM study of the various fracture micromechanisms has been reported separately (Kaplan et al., 2004). This study extends and confirms the principal results reported here.

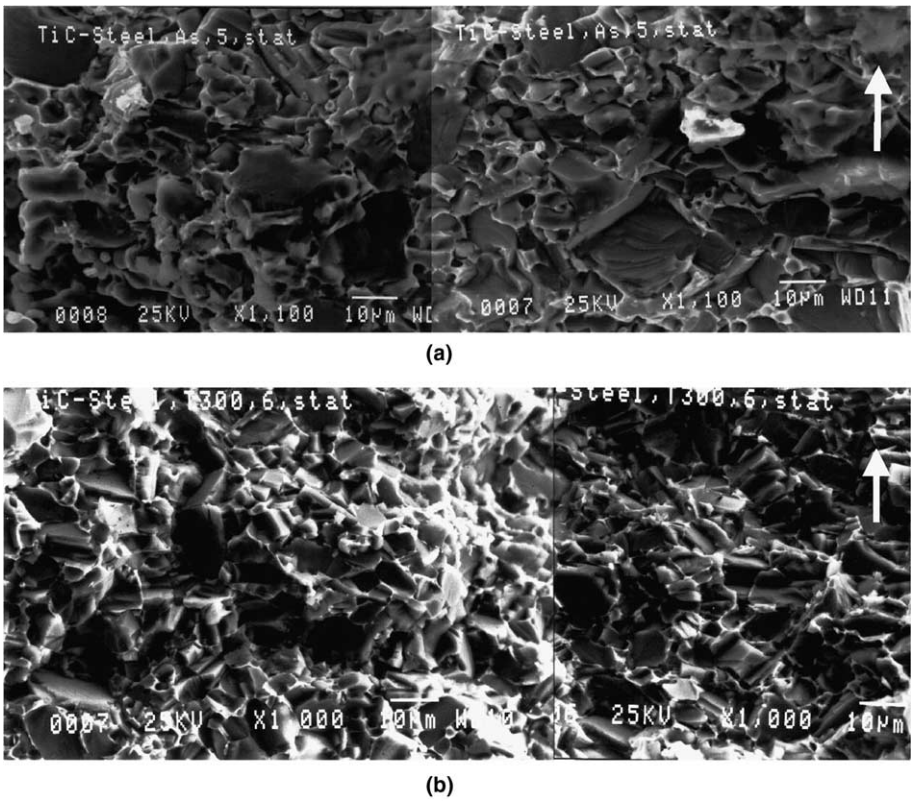

Fig. 9. Typical SEM fractographs taken in the vicinity of the starter notch. Room-temperature quasi-static fracture. The arrow indicates the direction of crack propagation. (a) AS and (b) T300.

5. Discussion

The present work investigates the static and the dynamic behavior of a TiC-1080 cermet, the steel matrix of which has been subjected to various heat treatments. The fracture behavior has been characterized, both in terms of fracture mechanisms and in terms of fracture toughness. The first point shows well defined operating fracture mechanisms, essentially cleavage of both the TiC particles and the steel matrix. These mechanisms are operative, irrespective of the thermal treatment of the cermet (steel matrix), the test temperature and loading rate. Therefore, at this stage, one cannot distinguish a definite failure mechanism that characterizes dynamic failure, as opposed to quasi-static.

Considering the quasi-static fracture toughness, the results obtained show that the various heats can be distinguished to some extent, indicating that the thermal treatment confers a superior toughness to the cermet as opposed to its as-infiltrated condition. Specifically, it appears that the Quenched and T300 conditions are the toughest of all four conditions investigated.

As a preliminary remark, it should be noted that all the fracture specimens contained sharp notches rather than fatigue precracks that are extremely delicate to grow in this kind of materials. Consequently, the reported fracture toughness values may be influenced to some extent by the finite root radius of the notch and should therefore be considered as ''apparent'' initiation toughness values. However, the very nature of the notch tip does not influence the results reported here since a systematic comparison is established between quasi-static and dynamic behavior of the same specimens.

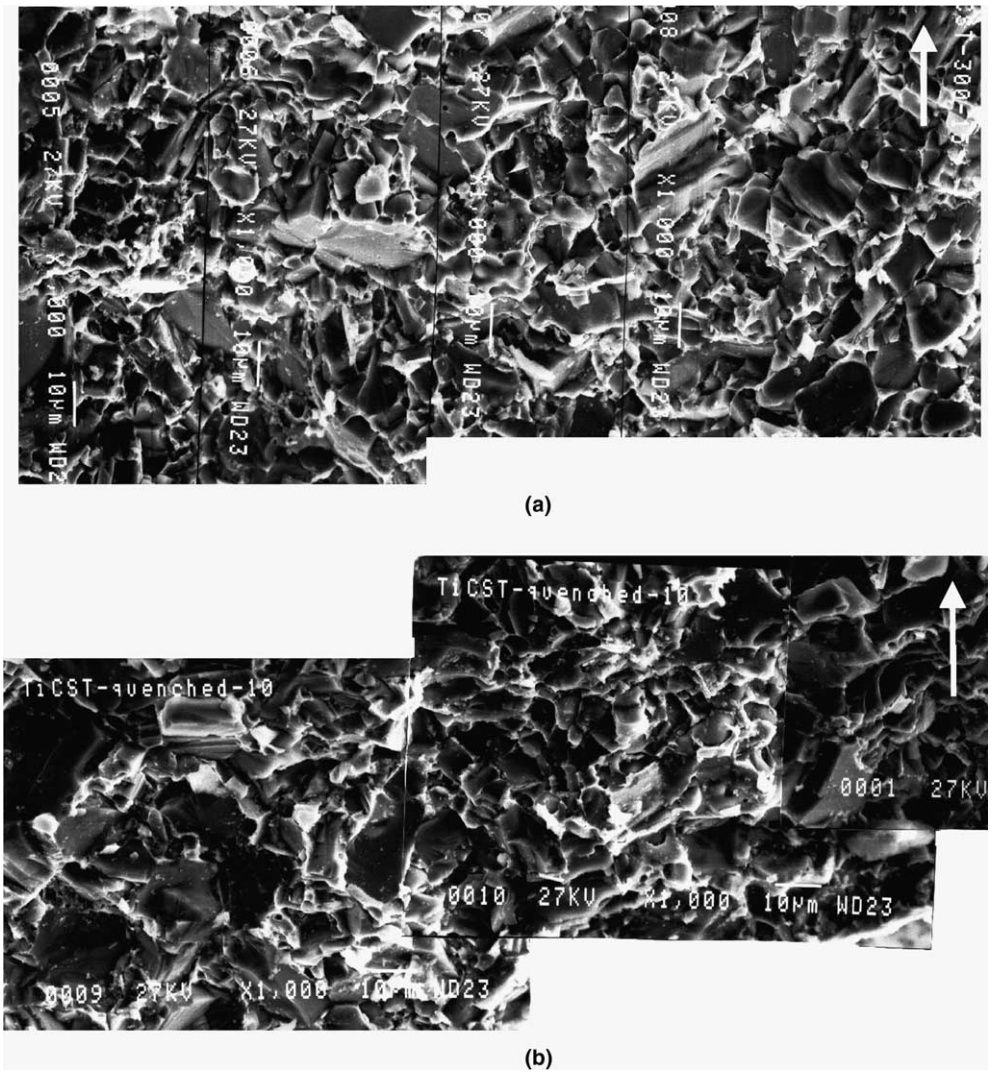

Fig. 10. Typical SEM fractographs taken in the vicinity of the starter notch. Room-temperature dynamic fracture. The arrow indicates the direction of crack propagation. (a) T300 and (b) Quenched.

A key result of the present investigation, which has not been reported in previous investigations of similar materials, concerns the *noticeable difference between quasi-static* (K_{Ic}) *and dynamic* (K_{Id}) *fracture toughness*. This point will be addressed in the sequel.

It is a well know fact that the dynamic fracture toughness can vary from the static one in monolithic materials. Variations of the fracture toughness with the loading rate can be explained with reference to the failure criterion, be it a local stress (to account for cleavage) or a local strain (to account for some ductile deformation, see e.g. Freund, 1992). From a mechanical point of view, for a stress controlled mechanism, the rate sensitivity of a given material (as this is the case at least for 1080 steel matrix, as many other steels (Meyers, 1994), should decrease its fracture toughness at high loading rates, on the basis of strain energy considerations. The same argument justifies an increase of fracture toughness with the loading rate

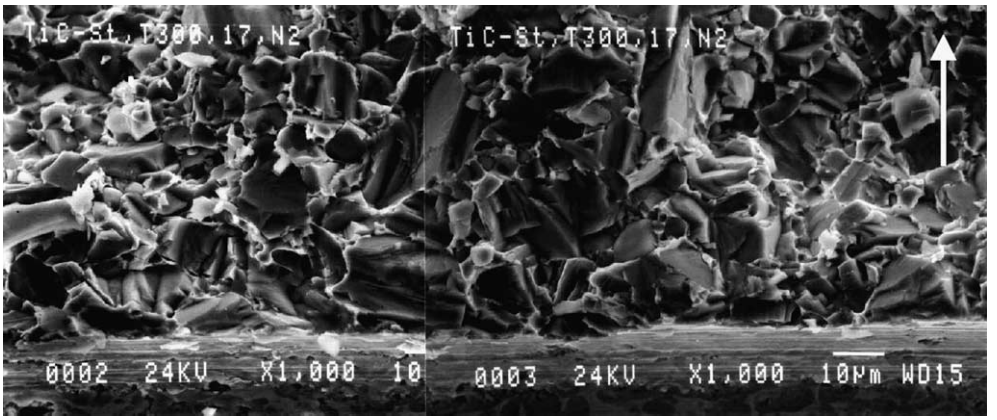

Fig. 11. Typical SEM fractographs taken in the vicinity of the starter notch. Low temperature quasi-static fracture. The arrow indicates the direction of crack propagation.

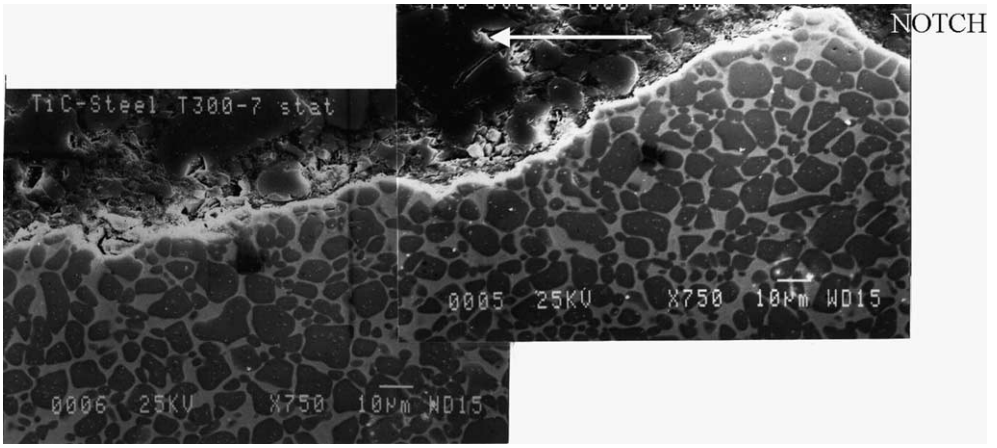

Fig. 12. Longitudinal section, taken at mid-thickness of a T300 specimen, perpendicular to the fracture plane. Quasi-static fracture. The thick arrow indicates direction of crack propagation. Note that the TiC grains and steel matrix below the fracture path are intact.

when a strain-controlled failure mechanism is operating. Identical conclusions were reached by Bodner (2001), based on a different viewpoint. In certain cases, the toughness variations are caused by a change of failure mechanism, as in a brittle to ductile transition. However, since the observed failure mechanism is essentially cleavage, one would expect a simple maximum normal stress criterion to yield dynamic toughness values that rank as described in Fig. 4. The results shown in Fig. 7 indicate that this is not the case, nor does the fracture toughness decreases with the loading rate. The observations just point to the opposite.

Another alternative consists of considering the rate sensitivity of a critical fracture stress, σ^*, as in Tetelman and McEvily (1967). The latter stress is considered to be temperature, and therefore rate independent. Low temperature testing can be regarded as equivalent to high strain rate testing. However, if σ^* were rate-sensitive, the low temperature experiments should have yielded quasi-static toughness values that are higher than the room temperature toughness. Here too, this was not the case.

Physically based micromechanical fracture models for particulate reinforced composites rely on the fracture micromechanisms. Sigl and Fischmeister (1988) described the toughness of cemented carbides in terms

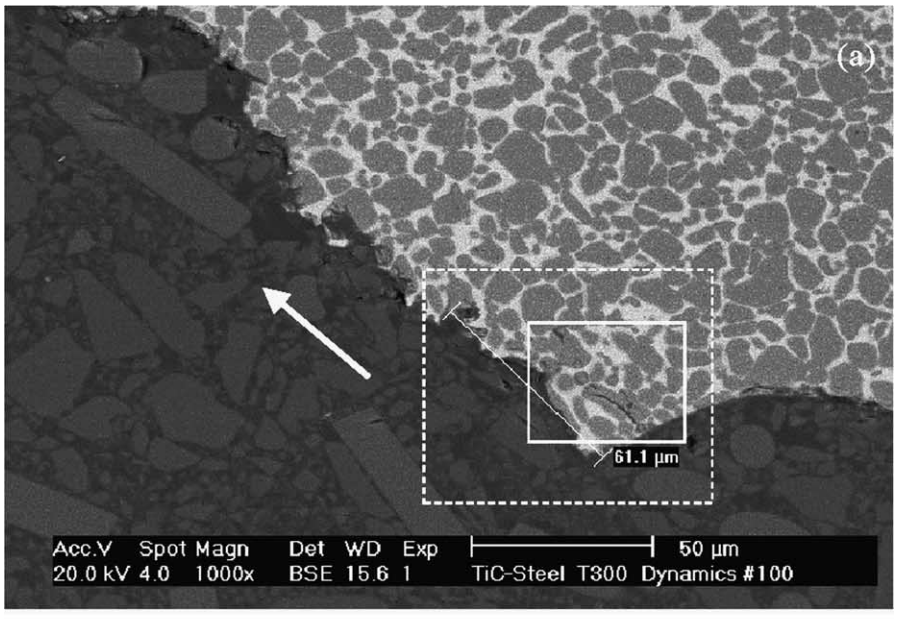

(a)

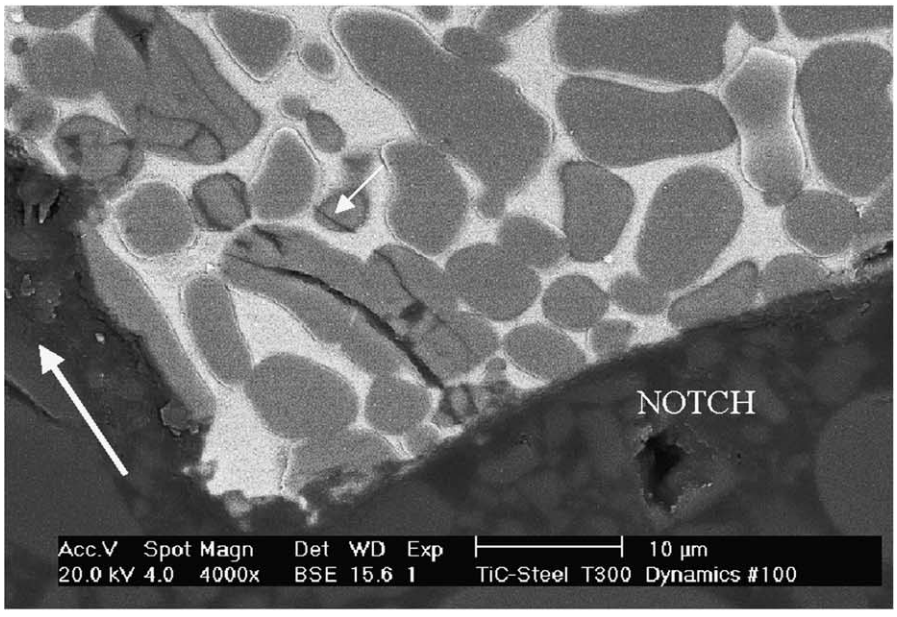

(b)

Fig. 13. Longitudinal section, taken at mid-thickness of a T300 specimen, perpendicular to the fracture plane. Dynamic fracture. The thick arrow indicates direction of crack propagation. (a) General view. The dashed frame indicates the damage zone. The smaller frame is magnified in (b). (b) Magnified backscattered electron image. Note the multiple cleavage cracks in the TiC grains (short arrow). No damage is apparent in the steel matrix. Damage is localized in an area, roughly 15 μm deep and 60 μm long.

of the various fracture paths and related fracture energies. Sigl et al. (1988) pursued the same line of investigation for a ductile reinforcement. Budiansky et al. (1988) analyzed in detail the small scale bridging effect

due to ductile particles, and toughening mechanisms were reviewed in Evans (1990) paper on high toughness ceramics. Various crack interaction schemes were examined by Kachanov (1993). This author investigated in detail the extent to which microcracks can actually shield a main crack, and the conclusion was that for three-dimensional cracks, large fluctuations of shielding and amplification may develop along the crack front. Consequently, a conservative approach would be to expect an overall amplification process due to elastic crack interactions of those microcracks that are closest to the main crack-tip.

However, all the above-mentioned results address cracks subjected to slowly varying loading. By contrast, dynamic fracture toughness modeling has been much less addressed from a micromechanical point of view. While the problem of the elastic crack interaction for dynamically loaded cracks is quite complex, some insight can be gained by considering the time t^* needed for Rayleigh waves to travel along a typical microcrack. A typical cleavage crack in a TiC grain is $l = 10$ μm long, and given the Rayleigh wave velocity $c_R = 6100$ m/s (Klein et al., 2003), $t^* = \frac{l}{c_R} \leqslant 2$ ns. A similar argument can be found in Espinosa (1994) who addressed the dynamic behavior of ceramic composites and their specific reaction to normal vs. pressure shear impact in terms of damage and microplasticity. Consequently the dynamic elastic interaction between microcracks is established in a very short time, so that a state of dynamic equilibrium is expected to prevail within the first microseconds of the wave loading. In this case, the above mentioned results of Kachanov (1993) must qualitatively apply to the present case. The case of a dynamically loaded crack surrounded by existing microcracks in a monolithic material has been investigated by Brockenbrough et al. (1988). Assuming that the microcracks are aligned parallel to the main crack, these authors got to the conclusion that microcracks do not significantly contribute to enhance the dynamic fracture toughness, unless their density is high and their velocity is extremely large (close to that of Rayleigh waves), in which case $K_{Id} \approx 1.7K_{Ic}$. The predictions of the model correlate with their experimental results, although it can be noted that for the assumed microcrack configuration, stress intensity amplification would be expected to occur rather than shielding. A key observation in this work was the similarity of fracture mechanisms in both quasi-static and dynamic fractured specimens, like in the present work. The authors did not characterize the nature of the damage underneath the main fracture plane as in the present work.

When considering the investigated cermet, one should keep in mind its specific microstructure consisting of two interpenetrated networks that was not investigated previous models. A thorough understanding of the failure micromechanisms is indeed a prerequisite to the understanding of the dynamic fracture response of these materials, as noted by numerous authors (Espinosa, 1994; Zavattieri and Espinosa, 2001; Espinosa and Zavattieri, 2003). Firstly, the toughening of the material, both static and dynamic, can be rationalized in terms of TiC cleavage cracks spreading to the tougher steel matrix. These mechanisms occur in *both* static and dynamic loading configurations, as evidenced from the fractographic analysis that does not differentiate between the two. Static failure of the two networks develops over a well defined fracture plane without additional damage. For the dynamic case, the observations of a crack-tip damage zone provide a snapshot of the situation prevailing immediately prior to completion of final fracture, as they outline the toughening role of the steel phase as a barrier to the spreading of TiC cleavage cracks. This interesting observation of early TiC cleavage is easily understood by considering the reported spall strength values of Klein et al. (2003), that are of 0.24 GPa for the TiC and of an average of 2.5 GPa for the steel matrix. This difference of one order magnitude in strength justifies the fact that the damage is essentially confined to the TiC particles. Our observations show that toughening cannot be ascribed to running microcraks as these are arrested at the steel-ceramic interface. Rather, the toughening factor is due to the formation of numerous microcracks in the damage zone, and the critical stage leading to final failure consists spreading of these microcracks into the surrounding steel matrix. Here, one should also mention the very interesting result of Ravichandran and Subhash (1995) that predicts strain rate sensitivity effects in ceramics using a model of non-interacting microcracks. Previous work has related the increasing number of cleavage microcracks below the main fracture plane to the increased impact toughness of a bainitic steel (Rittel et al., 2002b). The dynamic fracture toughness of a glassy polymer has also been noted to increase markedly with the loading

rate, with a noticeably rougher fracture surface topography that indicates multiple cracking in the immediate vicinity of the main crack (Rittel and Maigre, 1996). A similar point was made by Broberg (1999, 2002) about delocalization of damage for *running cracks*. Here, once a crack has reached a certain velocity, additional microcracking is likely to develop that is deemed to be responsible for the increased specific energy dissipation. Finally, a very recent numerical study of the influence of microcrack nucleation on dynamic crack growth in brittle materials has pointed to the very same result, namely that microcrack nucleation has a very significant influence of the energy dissipation for propagating cracks (Rafiee et al., 2004). This argument most likely applies also to the present case in which a main crack is rapidly accelerated into a damaging surrounding. Therefore, writing the quasi-static fracture criterion as $G_{\mathrm{Ic}} = -R_{\mathrm{o}}$, the dynamic fracture criterion will write as $G_{\mathrm{Id}} = -(R_{\mathrm{o}} + R_{\mathrm{extra}})$ in which G and R have the usual meaning of energy release rate and surface energy respectively. We believe that the damage zone formation, of dimensions $2 \times 60\ \mu\mathrm{m} \times 15\ \mu\mathrm{m}$, is likely to consume an additional finite amount of energy *prior to the onset of fracture*, R_{extra}, in view of the dominant volume fraction of the ceramic component. This increment of energy is deemed to be responsible for the increased dynamic fracture toughness of the investigated cermet.

6. Conclusions

This work investigates the dynamic mechanical properties and the fracture behavior of TiC-1080 steel cermets subjected to various heat treatments. As such, it is one of the few available studies on this subject. The main conclusions that can be drawn from the present study are:

1. Thermal treatments improve the dynamic strength of the cermet, with respect to the as-infiltrated condition.
2. The quasi-static fracture toughness, K_{Ic}, of the four conditions has been characterized. Conditions Quenched and T300 possess higher fracture toughness than the other two conditions.
3. The dynamic fracture toughness of all conditions, K_{Id}, is markedly greater than its quasi-static counterpart.
4. All heat treated conditions display relatively similar dynamic fracture toughness levels that are superior to the AS condition.
5. The failure micromechanisms of all conditions, irrespective of the test temperature and loading rate, consist essentially of cleavage of both the steel matrix and TiC particles, along with minor interfacial decohesion.
6. Dynamic loading induces a significantly higher level of localized damage around the crack-tip, as opposed to quasi-static loading. The damage consists essentially of cleavage of the TiC particles.
7. This observation is consistent with the relative spall strength of the TiC and 1080 steel components.
8. The observed fracture toughness increase with the loading rate is related to energy dissipation through TiC microcracking in the damage zone.
9. The critical microstructural fracture event is the spreading of cleavage microcracks in the TiC grains to the neighboring 1080 steel matrix.

Acknowledgments

This research was supported by the Israeli Ministry of Science under grant No. 20562-01-99. The Fund for Promotion of Research at Technion is also acknowledged for partial support.

References

ANSYS, 1994. User's Manual, Swanson Analysis Systems Inc.

Bodner, S.R., 2001. Unified Plasticity for Engineering Applications. Kluwer Academic/Plenum Publishers, Dordrecht.

Broberg, K.B., 1999. Cracks and Fracture. Academic Press, San Diego.

Broberg, K.B., 2002. Constant velocity crack propagation—dependence on remote load. Int. J. Solids Struct. 39, 6403–6410.

Brockenbrough, J.R., Suresh, S., Duffy, J., 1988. An analysis of dynamic fracture in microcracking brittle solids. Phil. Mag. A 58 (4), 619–634.

Budiansky, B., Amazigo, J.C., Evans, A.G., 1988. Small-scale crack bridging and the fracture toughness of particulate-reinforced ceramics. J. Mech. Phys. Solids 36 (2), 167–187.

Efron, B., 1979. Bootstrap methods: another look at the jackknife. Ann. Statist. 7, 1–25.

Espinosa, H.D., 1994. On the dynamic shear resistance of ceramic composites and its dependence on applied multiaxial deformation. Int. J. Solids Struct. 32 (21), 3105–3128.

Espinosa, HD., Zavattieri, P.D., 2003. A grain level model for the study of failure initiation and evolution in polycrystalline brittle materials. Part I: Theory and numerical implementation. Mech. Mater. 35 (3–6), 333–364.

Evans, A.G., 1990. Perspective on the development of high-toughness ceramics. J. Am. Ceram. Soc. 73 (2), 187–206.

Freund, L.B., 1992. Dynamic Fracture Mechanics. Cambridge University Press, Cambridge.

Kachanov, M., 1993. Elastic solids with many cracks and related problems. Adv. Appl. Mech. 30, 259–445.

Kaplan, WD., Rittel, D., Lieberthal, M., Frage, N., Dariel, M.P., 2004. Static and dynamic mechanical damage in TiC-1080 steel cermets. Scripta Met. and Mater. 51 (1), 37–41.

Klein, B., Frage, N., Dariel, M.P., Zaretzky, E., 2003. Dynamic response of ceramic-metal composites: The TiC-Steel system. J. Appl. Phys. 93 (2), 968–976.

Kolsky, H., 1963. Stress Waves in Solids. Dover Publications, New York.

Lifshitz, J.M., Leber, H., 1994. Data processing in the split Hopkinson pressure bar tests, Int. J. Impact Engng. 15 (6), 723–733.

Lloyd, D.J., 1991. Aspects of fracture in particulate reinforced metal matrix composites. Acta Metall. Mater. 39 (1), 59–71.

Metals Handbook, 1974. Fractography and atlas of fractographs, Vol. 9: ASM, Metals Park (OH), (see p. 181).

Meyers, M.A., 1994. Dynamic Behavior of Materials. J. Wiley and Sons, New York.

Parashivamurthy, K.I., Kumar, R.K., Seethamaru, S., Chandrasekharaiah, M.N., 2001. Review on TiC reinforced steel composites. J. Mater. Sci. 36, 4519–4530.

Rafiee, S., Gross, D., Seelig, Th., 2004. The influence of microcrack nucleation on dynamic crack growth—a numerical study. Eng. Fracture Mech. 71, 849–857.

Ramesh, K.T., Ravichandran, G., 1990. Dynamic behavior of a boron carbide-aluminum cermet: experiments and observations. Mech. Mater. 10, 19–29.

Ravichandran, G., Subhash, G., 1995. A micromechanical model for high-strain rate behavior of ceramics. Int. J. Solids Struct. 32 (17–18), 2627–2646.

Rittel, D., 2000. A note of the dynamic failure of PMMA. Int. J. Fracture 106 (2), L3–L8.

Rittel, D., Maigre, H., 1996. An investigation of dynamic crack initiation in PMMA. Mech. Mater. 23 (3), 229–239.

Rittel, D., Pineau, A., Clisson, J., Rota, L., 2002a. On testing of Charpy specimens using the one point bend impact technique. Exp. Mech. 42 (3), 247–252.

Rittel, D., Tanguy, B., Pineau, A., Thomas, T., 2002b. Impact fracture of a ferritic steel in the lower shelf regime. Int. J. Fracture 117, 101–112.

Rittel, D., Weisbrod, G., 2001. Dynamic fracture of tungsten base heavy alloys. Int. J. Fracture 212, 87–98.

Sigl, L.S., Fischmeister, H.F., 1988. On the fracture toughness of cemented carbides. Acta Metall. 36 (4), 887–897.

Sigl, L.S., Mataga, P.A., Dalgleish, B.J., McMeeking, R.M., Evans, A.G., 1988. On the toughness of brittle materials reinforced with a ductile phase. Acta Metall. 36 (4), 945–953.

Taya, M., Arsenault, R.J., 1989. Metal Matrix Composites. Pergamon Press, Oxford.

Tetelman, A.S., McEvily Jr., A., 1967. Fracture of Structural Materials. J. Wiley and Sons, New York.

Weisbrod, G., Rittel, D., 2000. A method for dynamic fracture toughness determination using short beams. Int. J. Fracture 104 (1), 91–104.

Zavattieri, P.D., Espinosa, H.D., 2001. Grain level analysis of crack initiation and propagation in brittle materials. Acta Mater. 49 (20), 4291–4311.